BAY OF FUNDY VERIFICATION OF A SYSTEM FOR MULTIDATE LANDSAT MEASUREMENT OF SUSPENDED SEDIMENT

John C. Munday, Jr.
Virginia Institute of Marine Science and School of Marine Science, College of William and Mary, Gloucester Point, Virginia 23062 U.S.A.

Thomas T. Alföldi
Canada Centre for Remote Sensing, 588 Booth Street, Ottawa, Ontario, K1A 0Y7 Canada

Carl L. Amos
Atlantic Geoscience Centre, Geologic Survey of Canada, Bedford Institute of Oceanography, P.O. Box 1006, Dartmouth, Nova Scotia, B2Y 4A2 Canada

Presented at: The Fifth Annual W.T. Pecora Symposium on Satellite Hydrology, Sioux Falls, South Dakota, June 11-14, 1979
Published in: "Satellite Hydrology", by the American Water Resources Association, 1979, pp. 620-640
Downloadable copy at: www.ccrs.nrcan.gc.ca\ccrs\eduref/ref/biblioe.html

ABSTRACT:

A system for automated multidate Landsat CCT MSS measurement of suspended sediment concentration (S) has been implemented and verified on nine sets (108 point) of data from the Bay of Fundy, Canada. The system employs "chromaticity analysis" to provide automatic pixel-by-pixel adjustment of atmospheric variations, permitting reference calibration data from one or several dates to be spatially and temporally extrapolated to other regions and to other dates. Correlation between a Landsat "chromaticity coefficient" and $\log_e S$ was $r = 0.965$, which produced a mean standard error of prediction of 30 percent of S. For verification, each data set was used in turn as test data against the remainder as a calibration set: the average absolute error was 44 percent of S over the range $1 < S < 1000$ mg/l. Effects of sediment type and size were negligible. The effect of solar angle was negligible except near the Brewster angle. The system can be used to measure chlorophyll (in the absence of atmospheric variations), Secchi disc depth, and turbidity. In a study related to the Fundy Tidal Power Project, S contour maps were used to initialize and calibrate a numerical model, and were also interpreted in order to define sediment transport paths and hydrodynamic flow. Results indicate that no significant sedimentation is expected from the proposed Fundy tidal barrage during its design lifetime.

(KEY TERMS: atmospheric variations; Bay of Fundy; Landsat; numerical model; suspended sediment; water quality.)

INTRODUCTION

Landsat measurement of aquatic suspended sediment can be very useful to many water quality monitoring programs and engineering studies. It is a practical and economical method for repetitive measurements in large and/or numerous water bodies. Furthermore, Landsat data are inexpensive. Appropriate data reduction techniques for Landsat measurement of suspended sediment have been sought by many authors since the launch of Landsat in 1972. One very recent study aimed at universal methods appropriate for multispectral scanner data is that by Holyer (1978). Other studies have been referenced in our earlier papers.

This paper is a report of recent advances in our joint work which began in 1974. We describe a Landsat data reduction system which uses chromaticity analysis to adjust for atmospheric variations between dates of Landsat passes. The system has been implemented for

the measurement of suspended sediment, and verified on surface data from the Bay of Fundy, Nova Scotia.

The system has been used to study the distribution, transport, and deposition of suspended sediment in the Bay of Fundy, the site for a proposed tidal barrage designed to generate electric power. The distribution of suspended sediment mapped by Landsat was used to calibrate and initialize a numerical model of post barrage siltation. Also, the transport paths of suspended sediment and the general hydrodynamic character of the flow were determined by visual interpretation of mapped suspended sediment patterns.

THEORETICAL DEVELOPMENT

Remote sensing satellite data must be calibrated by means of surface information, but it is impractical to provide calibration for each scene. Therefore, calibration must be extrapolated from scene to scene. The extrapolation procedure must adjust for date-to-date (temporal) variations, and region-to-region (spatial) variations. Variations occur in solar elevation angle, atmospheric attenuation and path radiance, and extraneous factors in surface reflectance.

The spatial noise may be termed “patchiness”. It cannot be corrected by spatial extrapolation from one part of a scene to another (by, for example, dark pixel subtraction); instead, a pixel-by-pixel correction using information specific to each pixel is required. Of the temporal variations, those due to solar angle are regular and correction methods for their effects are under study.

The approach described here treats spatial and temporal noise simultaneously through a preprocessing transformation, total radiance normalization. The procedures are analogous to some features of chromaticity analysis of human colour vision, hence the term “chromaticity analysis” (Munday, 1974a, b).

Total radiance normalization involves the ratio transformations $x_i = N_i/\mathbf{\Sigma}N_i$, where x_i are “chromaticity coefficients” and N_i are Landsat multispectral scanner (MSS) band radiances. This transformation suppresses noise when all bands suffer radiance changes in the same proportion, while leaving spectral properties of the data unaffected (Munday and Alföldi, 1975). For water quality analysis, bands 4, 5 and 6 are selected, excluding MSS 7 because strong infrared absorption by water in this band precludes its utility for volume information except at very high constituent concentrations. The result is two independent coefficients, x_4 and x_5, which are henceforth called chromaticity x and chromaticity y. The x-y plane is referred to as a chromaticity diagram (Figure 1), with equal radiance point E at (x, y) = (0.333, 0.333). The azimuthal or angular dimension contains “hue” (dominant wavelength) information while the radial dimension from E contains “saturation” (spectral purity) information.

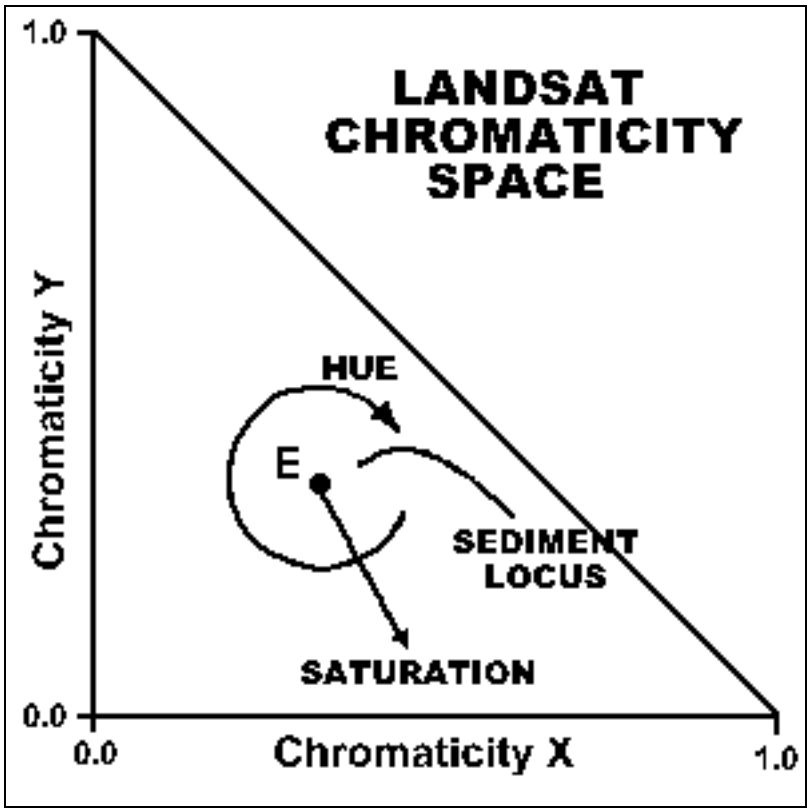

Figure 1: Landsat Chromaticity Diagram. "E" at (x, y) = (0.333, 0.333) is the "achromatic" point. From "E", azimuthal variation defines "hue", while radial distance represents "saturation".

The radial dimension is used to remove "desaturating" effects of environmental noise not suppressed by the chromaticity transformation itself. Atmospheric variations, thin clouds, air pollution, white caps, and thin snow and ice cover, all cause a radial shift of Landsat chromaticities toward "E" (Alföldi and Munday, 1977, 1978). This desaturating effect of the atmosphere is confirmed by studying atmospheric model data reported in the literature (Alföldi and Munday, 1978). Hence, a correction procedure for all the above variables involves simply a radial shift of chromaticities on the chromaticity diagram.

An attractive property of this noise correction technique is that it can be applied to new data lacking surface calibration, in order to standardize them to other data already calibrated. Consequently, a set of calibration data can be accumulated over any number of Landsat passes. In tidal estuaries, this feature is welcome because of the expense of obtaining surface data from dispersed locations within minutes of an overpass. Also, a unique correction is applied to each pixel rather than a scene wide correction. Both patchiness and temporal variations are thus corrected coincidentally. The result is that surface calibration of Landsat data can be extrapolated both spatially and temporally.

The chromaticity transformation and the subsequent radial shift of chromaticities remove two degrees of freedom from a multispectral data set. For the three band set of MSS 4, 5 and 6, one degree of freedom remains for correlation with water quality parameters.

The bulk of our work has been with suspended sediment measurement (Amos, 1976; Amos and Alföldi, 1979; Munday and Alföldi, 1979); equally satisfactory results are indicated for measurement of chlorophyll, Secchi disc depth, or turbidity. Some preliminary results for the latter variables are given below.

PROCEDURAL DETAILS

The sequence of data reduction steps is outlined in Table 1. The first step is conversion of

Data		Transformation	
Item	**Definition**	**Transform Function**	**Explanation**
D_4 D_5 D_6	Landsat MSS digital values (0-255) for bands 4, 5, 6		
		(Step 1) $R_i = a_i D_i + b_i$ I = MSS bands 4,5,6	a_i, b_i are prelaunch radiometric calibration constants for each Landsat
R_4 R_5 R_6	Radiance values (mw/cm^2-sr) for bands 4, 5, 6		
		(Step 2) $x = R_4/\Sigma R_i$ $y = R_5/\Sigma R_i$	Total radiance normalization.
x, y	Chromaticity coordinates		
		(Step 3) $x' = x + \Delta x$	
		$\Delta x = P_0 + P_1\theta + P_2\theta^2$ θ = projection angle	Atmospheric adjustment for x values. Radial projection of object locus onto reference locus to obtain x as a function of angle θ around E.
x', y'	Atmospherically adjusted chromaticity coordinates		
		(Step 4) $S = e^{m x' + b}$	Regression of water sampling data with satellite data.
S	Suspended sediment concentration (mg/l)		

TABLE 1:
Chromaticity Analysis of Landsat MSS Data for Suspended Sediment Concentration Measurement.

MSS band digital data numbers from Landsat computer compatible tapes (CCTs) into radiances using Landsat sensor calibration factors (NASA, 1976; Ahern and Murphy, 1978). For each band, the digital number used is an average of numbers from a 4 x 6 pixel area. This averaging suppresses residual MSS striping effects and recovers additional radiometric resolution. The second step is the chromaticity transformation. Chromaticities of turbid water bodies consistently form a curvilinear locus on the chromaticity diagram as shown on Figure 1. The end of the locus nearest E refers to the most turbid water. Under very clear atmospheres, the locus is found furthest from E; hazy atmospheres cause the entire locus to be projected toward E.

By plotting the chromaticity values of Landsat data which represent a ***range*** of suspended sediment concentration (S) values, the atmospheric homogeneity of the scene in question may be determined. A single atmospheric function is valid only for an area with a homogeneous atmosphere. By plotting data from another scene on the same diagram, the relative locations of the two loci will dictate the need to atmospherically "adjust" one locus to another.

From a series of loci developed in this manner from different regions and different overpass dates, a "standard' locus is selected. The most important selection criteria are that the standards locus include a large range of S, and that shifts of other loci to the standard locus be minimal in magnitude (Alföldi and Munday, 1977).

Step number three is the shift of loci for atmospheric adjustment. This adjustment is done, not for each point separately, but for a whole locus of points, preserving the width of the locus and the relative orientation of the points with respect to each other. This is accomplished by first curve fitting each locus by a second degree polynomial between x and y. Then the Δx component of the radial difference between the two polynomial functions is obtained as a function of angle θ around the point E. For this calculation, the angle θ is sampled at intervals of two degrees. The resulting pairs of values for Δx and θ are curve fit by a second degree polynomial, which is then used to calculate the specific x-coordinate correction for each point on the locus needing atmospheric adjustment. The adjusted coordinates are denoted as (x', y'). It is important to note that the atmospheric adjustment is based not only on the S-calibrated chromaticities, but on the full range of chromaticities in the calibrated water body (extracted with the aid of visual examination of CCT data).

Occasionally, there are anomalies in the relative positions of loci which are unrelated to atmospheric variations. Figure 2 is a plot of curve fit polynomials for nine Bay of Fundy loci. The loci were extracted from different parts of the Bay of Fundy over several pass dates, and thus represent both temporal and spatial variations. Curve 1 was chosen as the reference locus. Atmospheric adjustments were executed for curves 3, 5, 6, 7, 8 and 9 in the prescribed manner. For curve 6, extended radially toward E, the range of S was very small, between 1 and 3 mg/l, and hence the radial distribution is due to atmospheric variation. The remaining curves, 2 and 4, have deviant positions, and neither curve was adjusted; the curves suffered not a radial shift but a shift in y. Such anomalous shifts are not due to the atmosphere, because they occur only between scenes, not within scenes, while atmospheric shifts are radial and occur both between and within scenes. Such shifts can occur if the Landsat sensors suffer radiometric calibration drifts; for example, a decrease in the effective full scale radiance calibration factor in band 5 would cause chromaticities to be projected toward the x-axis along projection lines from the vertex (x, y) = (0, 1). Other possible causes of anomalous shifts are changes in the distribution of sediment with depth, dissolved pigmentation, and solar angle effects. Sediment types do not cause the anomalous shifts; however, residual solar angle effects may be present; both are discussed below.

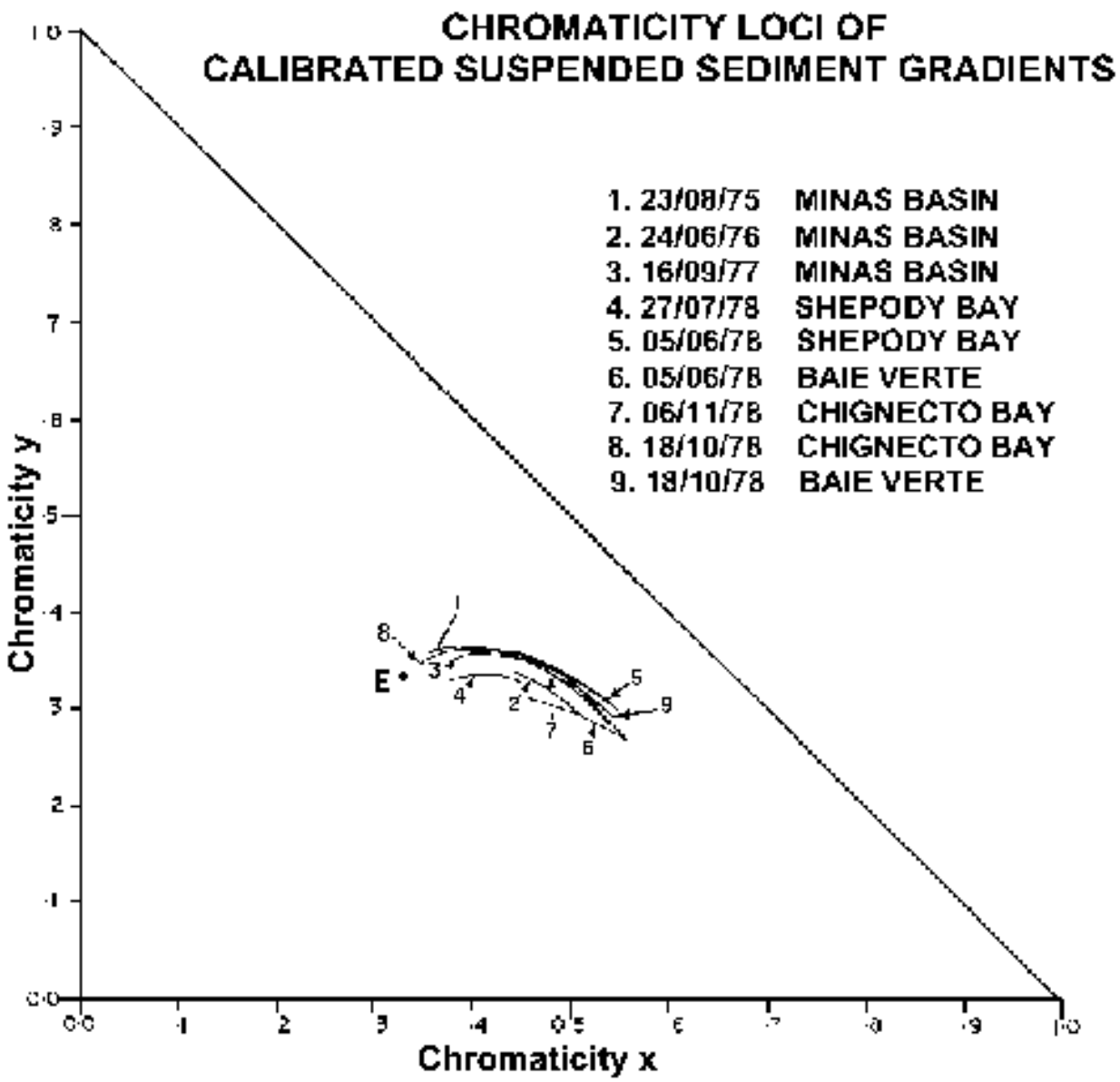

Figure 2. Chromaticity Loci of Calibrated Suspended Sediment Gradients. Locus No. 1 is used as the reference, loci No. 2 and No. 4 show anomalous shifts in y. Locus No. 6 shows atmospheric variability for a constant sediment concentration.

The fourth and last data reduction step is a regression between adjusted chromaticities and the suspended sediment concentration (S) data. After atmospheric adjustment, there remains one degree of freedom in the data; it is taken as x′ and regressed against $\log_e S$. The logarithmic relationship between x′ and S, discussed in Munday and Alföldi (1979), has been found valid for the range of 1 mg/l to 1,000 mg/l. All available S data from different Landsat passes may be used in the regression, or a portion may be used, as selected by the user.

The final stage of chromaticity analysis is the application of this regression to determine values of S for selected scene locations and/or to map S distributions. If a new CCT is to be used

at this stage, a locus from the new scene must be extracted and a correction polynomial $\Delta x = f(\theta)$ must be generated. Then, for scene locations of interest, x and θ are calculated, Δx calculated from the correction polynomial, x' found from $x' = x + \Delta x$, and S finally calculated from an inversion of the regression equation which relates x' and $\log_e S$.

SYSTEM IMPLEMENTATION

A suite of computer programs has been developed for the quantitative mapping of S from Landsat CCTs using chromaticity analysis. The programs are highly user interactive, involving cued sequences and user queries. The suite is implemented at the Canada Centre for Remote Sensing (CCRS) on the CCRS Image Analysis System (CIAS). Under a Canada – U.S.A. software exchange agreement, the suite has recently been transferred to the Eastern Regional Remote Sensing applications Center (ERRSAC) at NASA Goddard Space Flight Center.

CIAS performs digital image analysis based on a modified General Electric Company Image-100. The chromaticity suite does not use much of the specialized Image-100 signature analysis hardware, but it does exploit the capability of the PDP-11 control computer, and uses the interactive graphics and output capability of CIAS (the Image-100 colour television monitor, a Tektronix 4012 control terminal, a line printer, dot matrix printers, a thermal printer, and tape film transfer for photographic print output).

The programs (in Fortran) are arranged for construction and subsequent manipulation of two types of files: 1) chromaticity file containing both uncorrected and atmosphere adjusted chromaticities, and 2) calibration file containing corrected chromaticities and S values. Error statistics are computed automatically as described below. In the point mode, the user selects scene locations for S measurement using a joystick cursor, and the S value and standard error of prediction are automatically displayed on the colour television monitor adjacent to the cursor location. In the area mode, the scene is displayed with a colour code for S ranges, and a legend shows for each colour the mean S, S-range, number of pixels, and area in square kilometres. For a preselected segment of the scene, a histogram may also be displayed showing number of pixels versus S for the entire range of S. An example of area mode data is given in Table 2. A user familiar with the programs can map S distributions over a complete Landsat scene lacking surface data in under three hours. This time could be reduced significantly by batch processing, but at the expense of the interactive features which permit the analyst to exercise considerable control during data reduction.

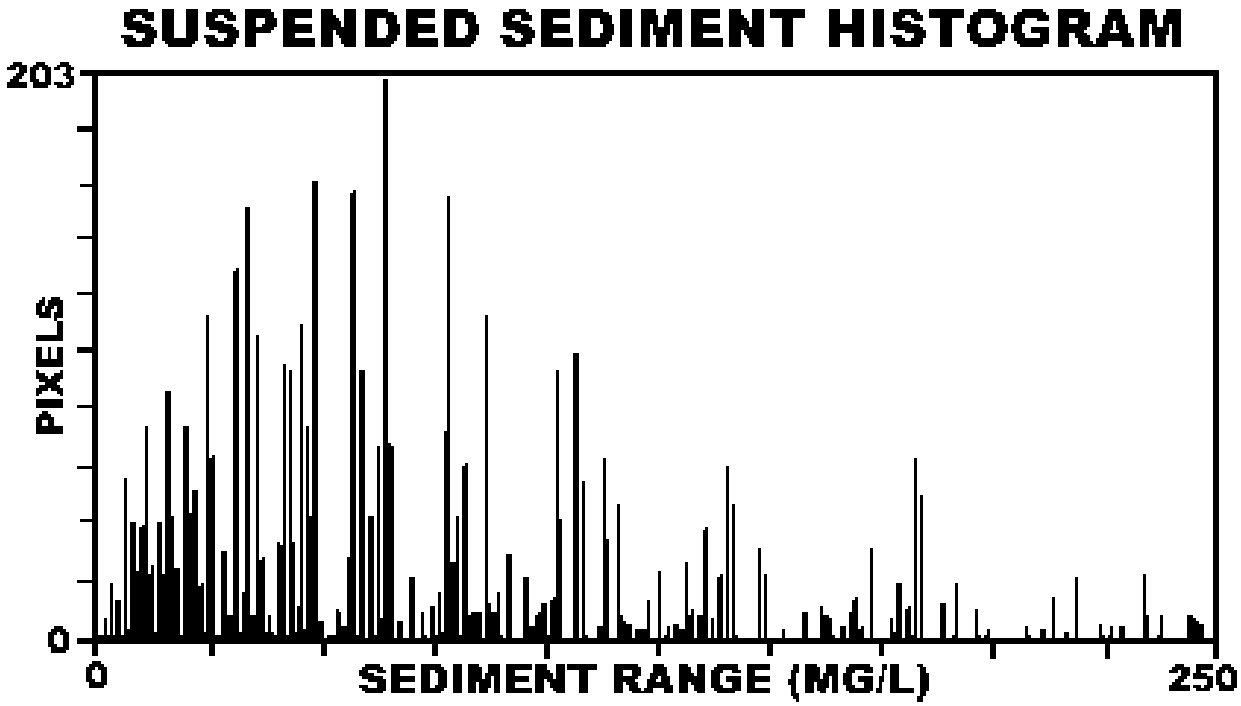

No. of Pixels (area) Analyzed	10449 (47.052 sq. km)
Valid Suspended Solids Limits	1 to 250
No. of Pixels (area) Outside Limits	5911 (26.617 sq. km)
No. of Pixels (area) Inside Limits	4538 (20.435 sq. km)
Mean Suspended Solids Concentration	73.089 mg/l
Standard Deviation	0.5311E + 02
Cursor Position	Top Left: (156, 36) Bottom Right (236, 164)

THEME MAPPING RESULTS

Theme	Low Limit	High Limit	Mean	Standard Deviation	Pixels	Area in Sq. Kilometres
0	AREA OUTSIDE LIMITS:				5911	26.617
1	1	2	1.56	0.4969E + 00	9	0.041
2	3	5	4.12	0.7221E + 00	43	0.194
3	6	13	9.66	0.2306E + 01	267	1.202
4	14	31	22.47	0.4994E + 01	717	3.229
5	32	73	50.34	0.1130E + 02	1691	7.615
6	74	173	109.20	0.2734E + 02	1485	6.687
7	174	250	200.92	0.2176E + 02	326	1.468

TABLE 2. Example of Statistics for Maps of Suspended Sediment Concentration.

COLLECTION OF SURFACE DATA

The calibration and subsequent discrimination of S using the chromaticity technique was initially undertaken in the Avon river Estuary, located in the Minas Basin system, Bay of Fundy (Amos and Alföldi, 1979). The calibration was thereafter extended to Chignecto Bay, Bay of Fundy and Baie Verte, Gulf of St. Lawrence. The locations of sample sites for each of the areas calibrated are shown in Figure 3. Nine data sets with a total of 108 surface samples have been obtained from seven passes of Landsats 2 and 3. Sample sites were marked by styrene floats

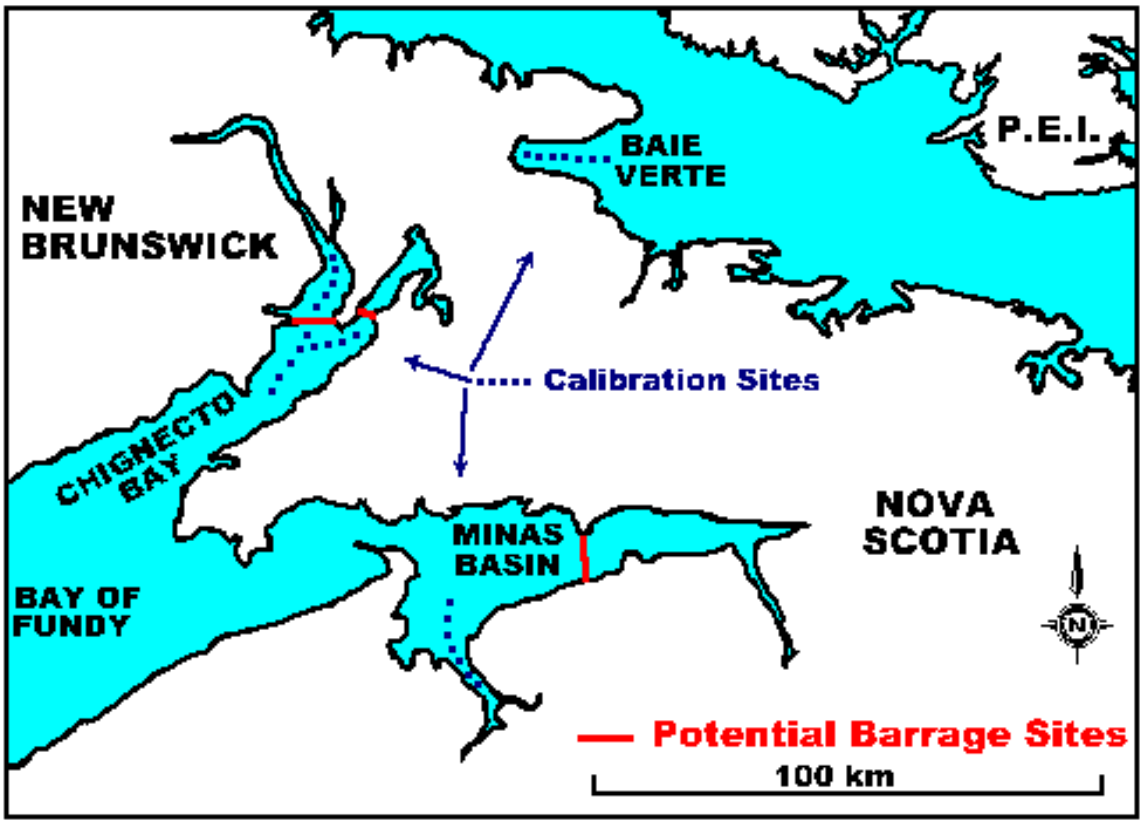

Figure 3. Bay of Fundy, Eastern Canada.

anchored approximately 1 km apart and at least 0.5 km from the low water shore. The floats were surveyed into position by sextant fixing on prominent coastal features, and resurveyed periodically to assess drift. The abundance of coastal features around the calibration site helped locate the sampling site on the Landsat imagery to within one 57 x 79 m pixel.

Samples were collected from a Bell Jet Ranger helicopter which hovered over each marked site at a height of 6 m. One litre surface water samples were collected using either Knudsen bottles or wide-neck Nalgene bottles lowered from the helicopter. In practice, one sample per minute could be collected using this technique.

The sampling time window was computed as: $T = \check{T} \pm L/\bar{U}$ where $\check{T}$ is the time of overpass on the previous satellite cycle, L is the Landsat sampling (spatial) resolution, and $\bar{U}$ is the mean tidal current speed at time $\check{T}$. The time window varied from 20 minutes to 6 minutes, decreasing as the tidal currents increased in speed. Within hours of collection, the samples were analyzed for:

1. Suspended sediment concentration (mg/l) determined by filtration through 0.45 μm Nuclipore filters (MacIntosh *et al*, 1976),
2. Chlorophyll *a* (mg/m^3), determined by fluorometry (Strickland and Parsons, 1972),
3. Grain size (microns), grain composition (elemental) and grain shape (Folk, 1968) measured directly from scanning electron micrographs, and
4. Selective absorbance of filtered and unfiltered water, using a Beckman 5 200 spectrophotometer.

The laboratory analyses of sediment concentrations have an accuracy of 1 mg/l. Twelve of the 108 samples have concentrations of sediment greater than 1,000 mg/l. Chromaticity x′ plotted against $\log_e S$ is shown in Figure 4.

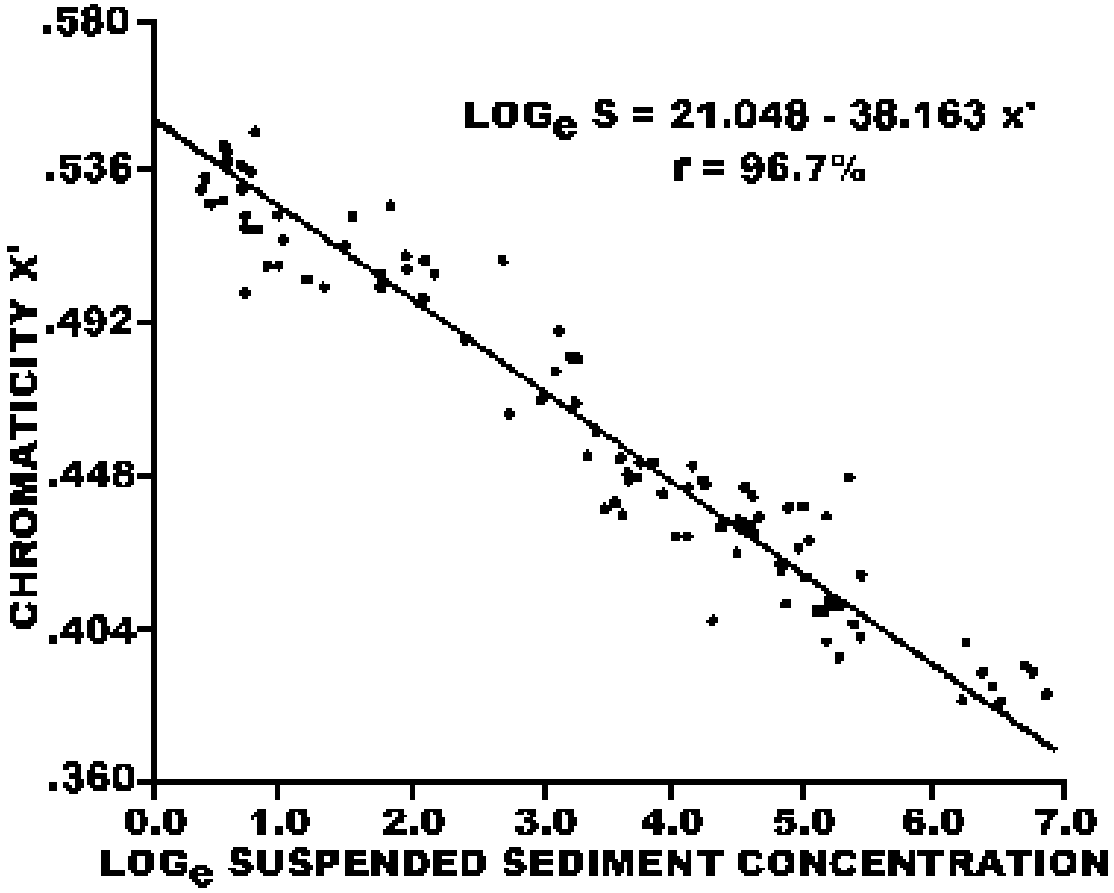

Figure 4. Sediment Calibration Function. x′ versus $\log_e S$ for nine data sets comprising 95 data points in the range $1 < S < 1{,}000$ mg/l.

SYSTEM VERIFICATION

Regression and Correlation Analysis

Model I linear regression between x′ and $\log_e S$ for the above data produces the equation $x' = 0.552 - 0.026 \log_e S$.
The Pearson product moment correlation coefficient r for this regression is 0.965 (see Table 3). (The Pearson statistic was used for convenience in comparison with the literature, acknowledging that its applicability may be questioned: there are insufficient radiance N values at each S value to permit a test of normality for N; also, some relationships involved are non-linear, such as the N-versus-S relation and atmospheric transfer; therefore, for a particular S value, the associated N values could be skewed.) Removing data at S > 1,000 mg/l, where N versus $\log_e S$ becomes nonlinear, yields r of 0.967 . Removing one data set a time and averaging the resulting r values yields r = 0.959 with a standard deviation of 0.01348 . These results indicate that neither data at S > 1,000 mg/l nor any single data set has an unduly large influence on the results.

TABLE 3. Correlations Between Landsat Data and $\log_e S$. Nine Data Sets (108 samples), Landsat-2 and –3, Pearson Correlation Coefficients.

MSS Band or Band Ratio	r
4	0.690
5	0.865
6	0.817
4/5	0.867
4/6	0.892
5/6	0.487
4+5+6	0.804
5*	0.844
x	0.955
y	0.599
z	0.848
x′	0.965

* Cosine solar correction

Results with x instead of x′ give an r of 0.952 . For removal of one data set at a time, the average r is 0.951, with a standard deviation of 0.00733 . Since all r values for x′ are higher than their counterparts for x, the atmospheric adjustment procedure produces a small improvement over unadjusted chromaticities, reducing the error by up to 5 percent.

Results with MSS 5 radiance values instead of chromaticity values yield an r of 0.818 . For one set removal, the average r is 0.821, with a standard deviation of 0.0241 . Comparison of all the above r values shows that the chromaticity transformation with atmospheric adjustment produces substantial correction for environmental noise.

Predictive Error

The statistical standard error of prediction associated with measurement of S from the Bay of Fundy data can be determined from

$$Error = \pm t_{(0.05,\, n-2)} S_{y \bullet x} \sqrt{\frac{1}{m} + \frac{1}{n} + \frac{(X - \overline{X}_i)^2}{(X_i - \overline{X}_i)^2}}$$

where X is the point estimate of $\log_e S$, $t_{(0.05,\, n-2)}$ is the t-statistic at the 95 percent confidence level, $S_{y.x}$ is the root mean square deviation from regression, m is the number of pixels averaged for each point measurement, n is the number of samples, and

$$X_i \text{ and } \overline{X}_i$$

are the point and mean values of $\log_e S$ (Sokal and Rohlf, 1969). The resulting confidence limit ΔS as a function of S is shown in Table 4. The second degree polynomial curve fit to these data

TABLE 4. Belt of Estimated Error at 95 Percent Confidence for Prediction of S.			
S (mg/l)	Log_eS	Error Belt (percent)	
1.0	0	24.0	31.0
2.7	1	21.7	27.6
7.4	2	20.0	25.2
20.1	3	19.4	23.9
54.6	4	19.5	24.2
148.4	5	20.4	25.7
403.4	6	22.1	28.3
1096.6	7	24.2	32.1

shows errors are smallest in the midrange of S, as expected. The standard error of prediction (95 percent confidence limit) is seen as roughly 25 percent of the value of S throughout the range 1 mg/l to 1,000 mg/l. Such an error in S is expected when r for log_eS is about 0.96 .

Absolute Error

The absolute error of the regression was determined by using, in turn, each set of data as a test against the other eight sets as training data. The data for S > 1,000 mg/l were removed before these computations. The error so determined are true absolute errors. The nine sets of errors are collected on one graph in Figure 5. In this presentation note that the same data are used

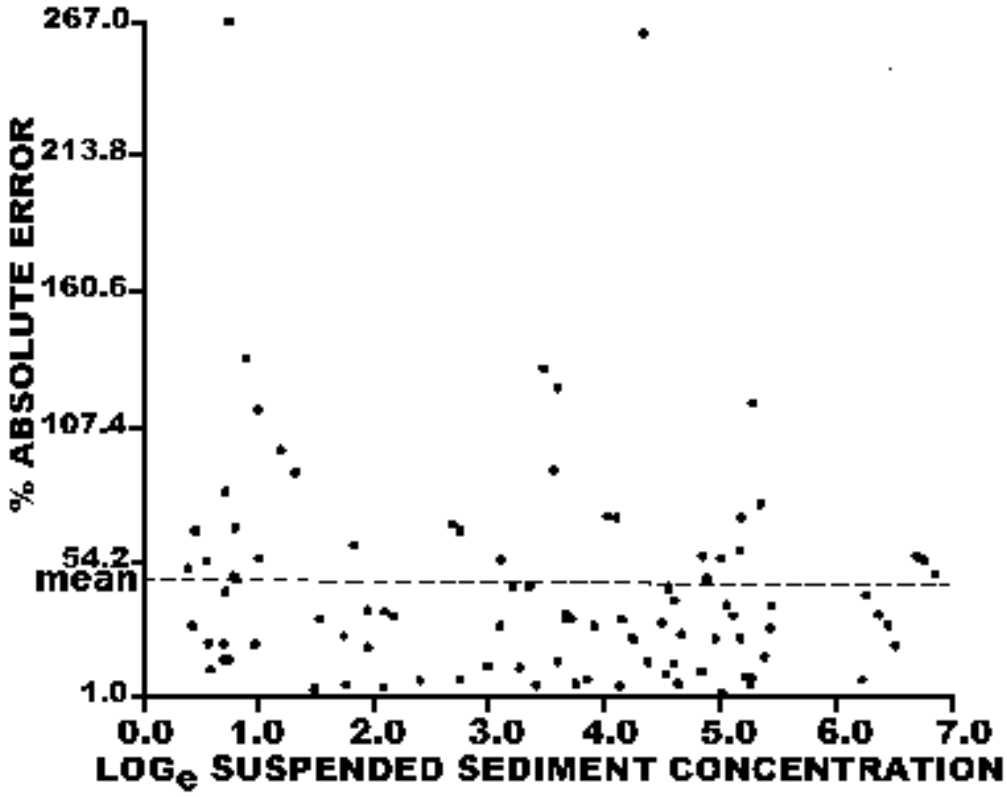

Figure 5. Absolute Error of Calibration. Each of nine data sets is compared against the composite of the other eight. Mean absolute error: 44 percent.

repeatedly. The mean error is 44 percent. The accuracy required by the U.S. Environmental Protection Agency for monitoring suspended sediment is defined as a variance not to exceed 0.05 (Holyer, 1978). The corresponding percent error in S is 23 percent. Results here are outside the U.S. EPA standard.

Error Analysis

One source of error is Landsat system noise. An rms sensor noise of ± 1 digital count in each band would result in errors (under chromaticity analysis of ***single pixels***) of 100 percent at low S values. Note, however, that errors of similar size from system noise would be obtained with all Landsat methods of S measurement. The system noise error is diminished by the 4 x 6 pixel averaging.

A second error source is associated with inhomogeneous distribution of suspended sediment in water. This error is inherent in all data collection, whether for single of multiple dates. The greater the within pixel inhomogeneity, the worse the error. Inhomogeneity has two effects: first, the collected sample may not be representative of the "average" sediment concentration in the field of view; second, due to nonlinearity between radiance and S, increasing inhomogeneity in the distribution of a given amount of sediment results in a worsening underestimate of its average concentration in the field of view. The magnitude of these effects on total error for Bay of Fundy data cannot be evaluated because of lack of appropriate data; it would depend on the particular spatial distribution of suspended sediment.

Owing to uncertainties in the magnitudes of the above errors, discrimination of the residual error from uncorrected atmospheric variability is uncertain. In any comparative evaluation of atmospheric adjustment techniques, a measure of absolute error (see above) can be used to test the *total impact* of techniques on S measurement.

THE EFFECTS OF SEDIMENT SIZE AND COMPOSITION

Detailed results of the effects of sediment size and composition are available from the Minas Basin (Figure 6) where S values ranged from 1.97 mg/l to 79.48 mg/l. The percentages by

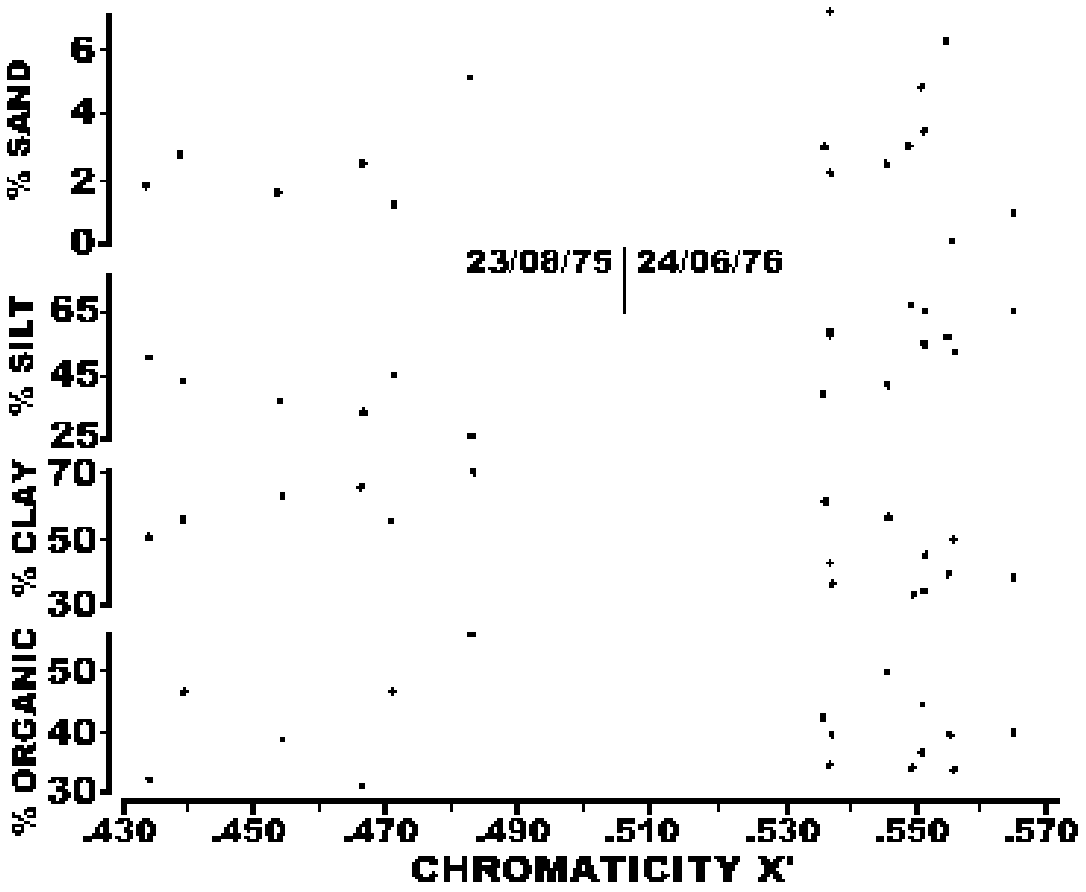

Figure 6. Sediment Size Distribution Related to Chromaticity x´. Sand + silt + clay = 100 percent; percent organic determined by weight loss on ignition at 600^0C. Size fractions and organic content have no relationship with chromaticity x´.

surface area of sand plus coarse silt (> 32μm), silt (4-32μm), clay (< 4μm), and organic content are plotted in Figure 6 for each of the samples from the Minas Basin. The percentages are based on (SEM) microscopic examination and represent the *in situ*, flocculated size distribution. Under rough conditions (August 23, 1975), sand size material up to 800μm in diameter was found in suspension (Figure 7D) together with benthonic foraminifera (Figure 7C) and large diameter floccules of clay material (Figure 7A). Under calm conditions (June 24, 1976), small diatoms (Figure 7B), clay particles, and 30μm floccules predominated.

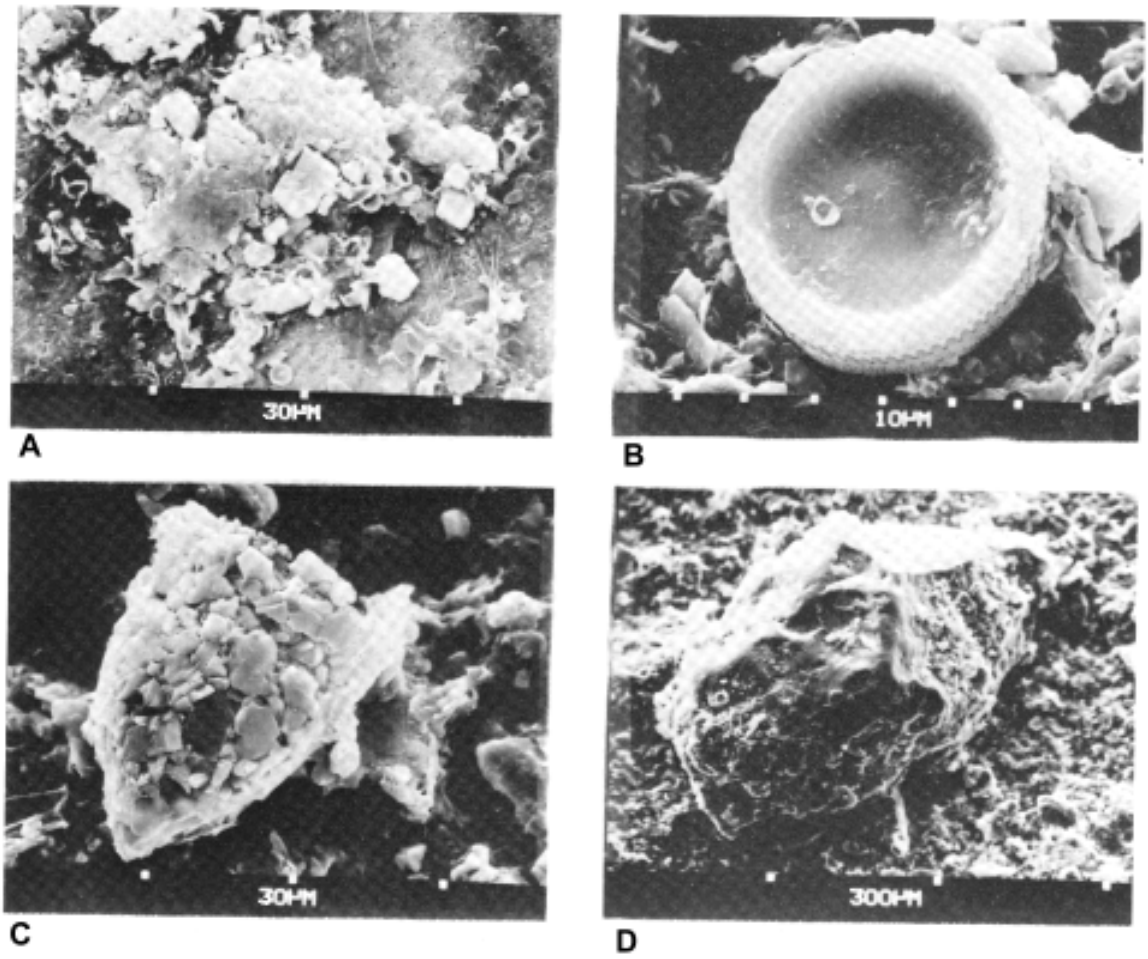

Figure 7. Four Scanning Electron Microscope (SEM) Images of Suspended Material From the Minas Basin, Collected in Rough Sea Conditions: (A) a floccule of clay material; (B) a diatom frustule; (C) a benthic, agglutinated foraminifera; (D) a siliciclastic particle of sand

Chromaticity x´ is plotted in Figure 6 against sediment size and type. Chromaticity shows significant variations between differing dates of sampling, corresponding to differing S levels only. The percentage clay for a constant chromaticity x´ value varies from 32 to 60. Samples containing 49 percent clay, on the other hand, show chromaticity x´ variations from 0.434 to 0.556, which represents most of the calibration range. The percentage silt varies from 25.8 percent to 66.6 percent and sand varies up to 7.1 percent. Again there is little relationship with the chromaticity coordinates. These results indicate that grain size does not affect the chromaticity calibration to S.

The percentage organic matter, recognized as shell debris, sponge spicules, diatom frustules, egg sacks, foraminifera, radiolaria and lignaceous matter, varies from 30.9 percent to 54.2 percent of total suspended sediment. The organic materials show a wide variety of differing shapes, sizes, and surface textures, quite different from the inorganic floccules of clay or the

siliciclastic particles (Figure 8). Yet, as can be seen in Figure 6, chromaticity appears to be independent of such variations. Backscatter, of which Landsat radiance is a measure, is indeed a function of grain size and shape (Jerlov, 1976). However, to the extent that grain size and shape cause radiance changes in all bands in the same proportion, the chromaticity transformation compensates for these effects.

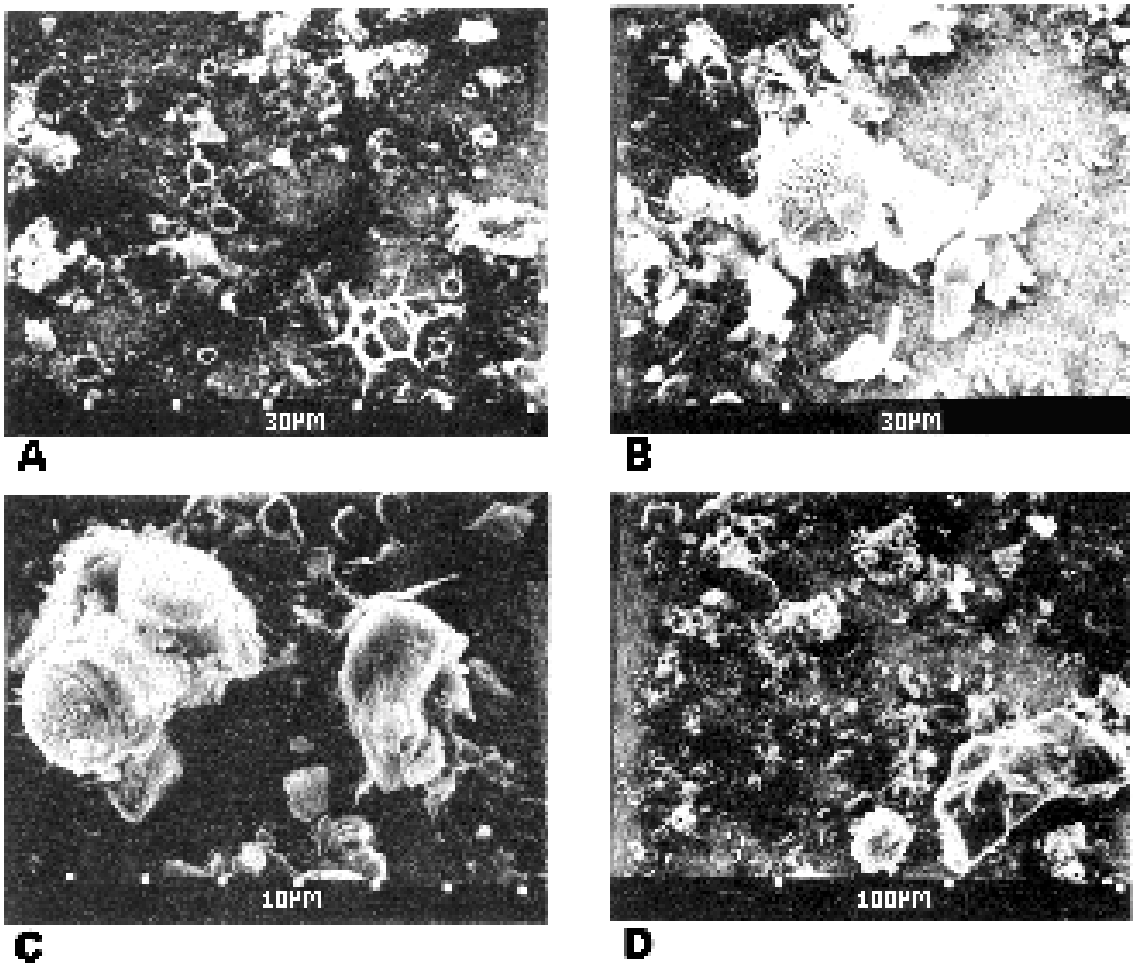

Figure 8. Four Scanning Electron Microscope (SEM) Images of Suspended Material From the Minas Basin, Collected in Calm Sea Conditions: (A) egg sacks and a radiolarian, (B) a diatom and diatom frustule fragments, (C) a composite floccule of diatoms and clay particles, and (D) a mixture of suspended particulate matter.

An initial examination of the sampled material from two other sites, Chignecto Bay and Baie Verte, shows it to be quite different from the Minas Basin material. Suspended sediment from Chignecto Bay has a unimodal distribution of sizes, peaking in the 8-16µm range. Flocculation, controlled by the source material, is much less and siliciclastic material dominates (85.8 percent to 100 percent). In Baie Verte, S is typically below 2 mg/l, and the majority of the matter is organic (32.1 percent to 71.1 percent). The siliciclastic particle size distribution is also unimodal here, peaking in the 8-16µm range. Despite obvious sites, the 45 data points from Chignecto Bay and Baie Verte did not appreciably alter the original Minas Basin calibration.

THE EFFECTS OF CHRLOROPHYLL

Regressions between chlorophyll concentrations and Landsat MSS radiances have been examined by Bukata, *et al.* (1974); Bowker, *et al*. (1975); Rogers, *et al.* (1975, 1976); Boland (1977), and Minnesota Region 5 (1978). Obviously, chlorophyll can have an effect on Landsat measurements of S, but how this effect varies with S is uncertain.

In the Avon River Estuary, the chlorophyll *a* concentration (C) is typically less than 0.5 mg/m^3, which according to Bukata, *et al*. (1974), is below the limits of detection by Landsat. In Baie Verte, C represented 0.4 percent to 0.7 percent of S (by weight), but the range of S in these samples was only 1.45 to 8.11 mg/l, so the relative effects of sediment and chlorophyll cannot be assessed. In Chignecto Bay, C varied from 1.14 mg/m^3 to 11.6 mg/m^3. These chlorophyll values represent only 1 part in 5.4×10^3 to 1 part in 14×10^6 of the total S (by weight). Therefore, the direct effect of C relative to the remaining S is considered insignificant. Even the associated biomass contributes negligibly to S measurement. This can be verified by simple estimation of the dry weight associated with such values. In data reported by Scherz (1977, pp. 150-158) laboratory algal cultures of three species had chlorophyll concentrations between 0.4 and 0.9 percent of dry cell weight, 15 mg/m^3 chlorophyll is associated with 1.5 mg/l dry cell weight, again an insignificant contribution to all but low S values.

Chlorophyll data published by other investigators have also been examined. In four sets of data from fresh water lakes, C appears to have been much larger relative to S than in the Bay of Fundy. The radiance data were converted into chromaticities, which are shown in Figure 9.

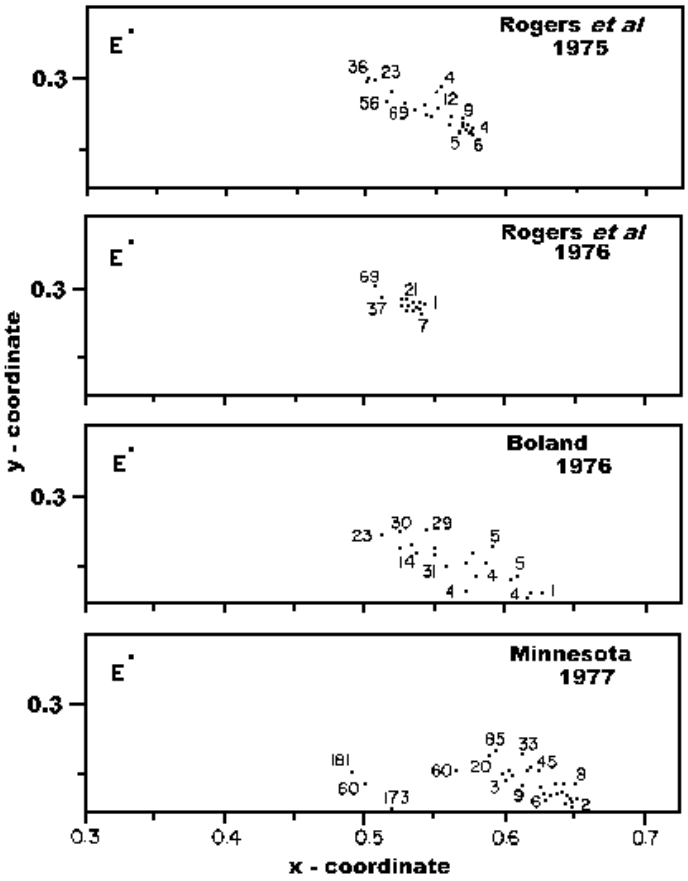

Figure 9. Chlorophyll Data From Other Sources, Plotted With Respect to Chromaticity Coordinates. Numbers are chlorophyll concentrations in mg/m^3 for individual data points.

The data are too sparse to permit a selection of the best chromaticity coordinate for regression against C, but the linear regression correlation coefficient between x and C for each data set was about 0.80 (Table 5). Also, because S data were not provided, the exact extent of influence of S on the C locus cannot be determined.

TABLE 5. Landsat Chromaticity Analysis for Secchi Depth and Chlorophyll *a* Concentration

Pearson Product Moment Correlation Coefficients

		Secchi Depth			Chlorophyll *a* Concentration		
Data Set*	Number Samples	Range (m)	Model	r	Range (μg/l)	Model	r
1	20	0.30 - 5.70	x vs. ln SEC 4/5 vs. ln SEC	0.89 0.92	0 - 30	x vs. ln CHL ΣN_i vs. CHL	0.88 0.90
2	34	0.27 – 3.20	x vs. ln SEC	0.90	2 - 181	x vs. CHL 6 vs. CHL	0.92 0.96
3	27	0.30 – 2.20	x vs. ln SEC x vs. SEC^{-1}	0.94 0.96	2 - 69	z vs. ln CHL 4/6 vs. ln CHL	0.79 0.81
4	16	0.60 – 2.20	x vs. ln SEC y vs. SEC^{-1}	0.79 0.91	1 - 69	y vs. ln CHL	0.92

* Sources: Boland, 1976; Minnesota Region 5, 1978; Rogers, *et al*., 1975; Rogers, *et al*., 1976.

NOTE: Highest correlation and highest chromaticity correlation shown. Correlations tested: 4, 5, 6, 7, ΣN_i, 4/5, 4/6, 4/7, 5/6, 5/7, 6/7, x, y, z.

Two conclusions concerning chlorophyll measurement are possible. First, for single dates, C measurement with chromaticity coordinates appears as accurate as with other measures on MSS radiance such as band ratios. Second, the locus with increasing turns toward E and at high values passes beneath E to the chromaticity region for vegetation at (x, y) = (0.3, 0.2). this behaviour renders the atmospheric adjustment technique inapplicable in the presence of high C, because the atmospheric adjustment technique also involves use of shifts toward E. Thus, the simultaneous measurement of S and C, together with multidate atmospheric adjustment, is not possible with the chromaticity system in its present stage of development. However, where chlorophyll bearing particles are the dominant component of suspended particulate matter, a single date measurement and mapping of chlorophyll should be reliable.

THE EFFECTS OF DISSOLVED ORGANIC MATTER

The effect of pigments dissolved in the sea water samples was assessed in an indirect manner by measuring the transmittance (τ) of light between the wavelengths of 400 – 800 nm and along a 10 cm path length. The transmittances were normalized to a standard 30 percent NaCl solution in distilled water. Fresh water samples from rivers debouching into the Bay of Fundy were compared with filtered and unfiltered sea water samples. The results are shown in Figure 10.

The filtered sea water samples show light transmittances of 95 percent, similar to distilled water; attenuation results from colloidal matter not trapped by the filtering process. The unfiltered sea water samples show τ less than 20 percent at 63 mg/l and less than 10 percent at 149 mg/l; here, the effect of S dominates. The transmittance curve of the fresh water, on the other hand, shows the effect of pigmentation. The relative attenuation at 400 to 500 nm is significant and is probably the result of dissolved organic matter. This fresh water pigmentation is diluted by the enormous tidal prism into which it flows. The conclusion based on these observations is that our results are not affected by dissolved organic matter.

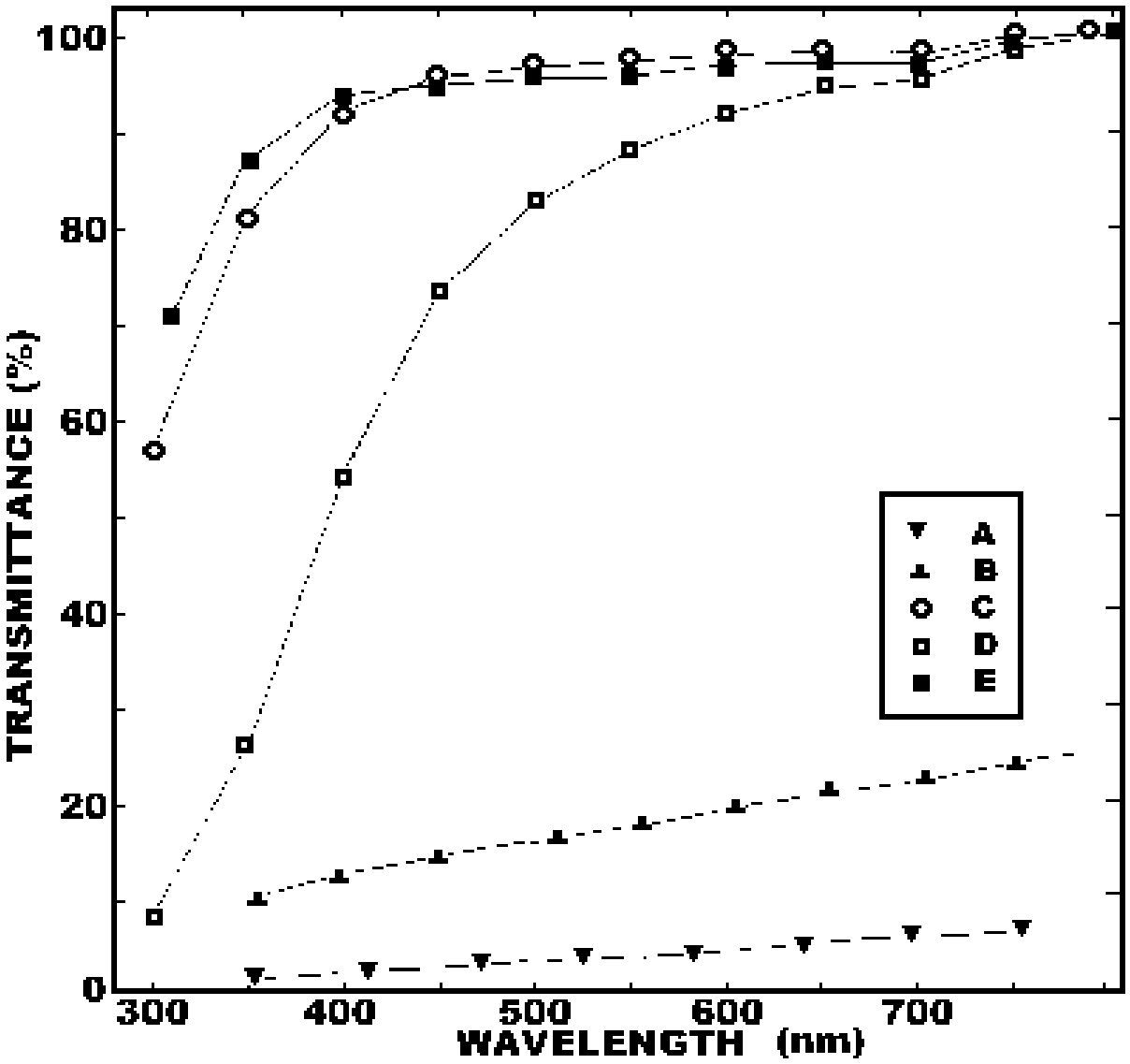

Figure 10. Spectral Transmission of Water Samples. Normalized to 30 Percent NaCl Solution in Distilled Water. Path length 10 cm, Beckmann 5 200 spectrophotometer – (A) unfiltered Chignecto Bay sea water at S of 149 mg/l, (B) unfiltered Chignecto Bay sea water at S of 64 mg/l, (C) filtered sea water from outer Chignecto Bay, (D) filtered river water from the Petitcodiac River, and (E) filtered sea water from inner Chignecto Bay.

THE EFFECTS OF SOLAR ANGLE

The high correlation coefficient between x' and $\log_e S$ for nine data sets ($r = 0.965$) indicates that the chromaticity technique with atmospheric adjustment accounts at least partially for variations in solar elevation angle. Moreover, the results are better than those for MSS 5 data modified by a cosine correction for solar angle. Recently published analysis of three of the data sets (Munday and Alföldi, 1979) shows that the chromaticity transformation, even without atmospheric adjustment, produces correlation coefficients as high as those from solar corrected MSS 5 data. For nine data sets combined, solar corrected MSS 5 data yield $r = 0.844$, a small

drop from uncorrected MSS 5 data, where r = 0.865. These MSS 5 r values are well below the r value for x´.

Nevertheless, there appears to be a residual (second order) effect of solar angle variations on the chromaticity diagram. The relation has been studied with a series of Landsat data for oligotrophic lakes. Stewart Lake, Nova Scotia, has been studied on eight Landsat images, and Cousin's Lake, Manitoba, has been studied on four passes. The oligotrophic character of these lakes ensures that their volume reflectance properties are constant with time. In earlier work, we reported that the chromaticity changes with time for these lakes were too large to be due to noise, and that the changes were likely due to changes in atmospheric haze from date to date (Alföldi and Munday, 1978, Figures 5a and 5b).

It is also possible that a portion of the changes results from changes in solar elevation angle, and the consequent change in both reflection geometry and irradiance spectrum. It can be expected, in general, that higher solar angle will shift the illumination toward shorter wavelengths. This shift should increase x and decrease y on the chromaticity diagram.

The chromaticity data for each lake were regressed against solar elevation angle. The procedure was to average the chromaticity data for each date and then analyze each average into components: 1) the azimuthal angle θ_E (relative to x, y = 0.7, 0.2) subtended at E, the equal radiance point; 2) the coefficient x; and 3) the radial distance from E (a measure of the Landsat "colour" saturation).

For Stewart Lake, correlation coefficients for all components were below 0.5 and failed to be significant at $P < 0.1$ (n = 8). The regression against solar angle of the sum of the components θ_E and d produced r = 0.71, significant at only $P < 0.1$. A plot of θ_E against solar angle (Figure 11) indicates that the point for 29 September 1973 was wild; hence,

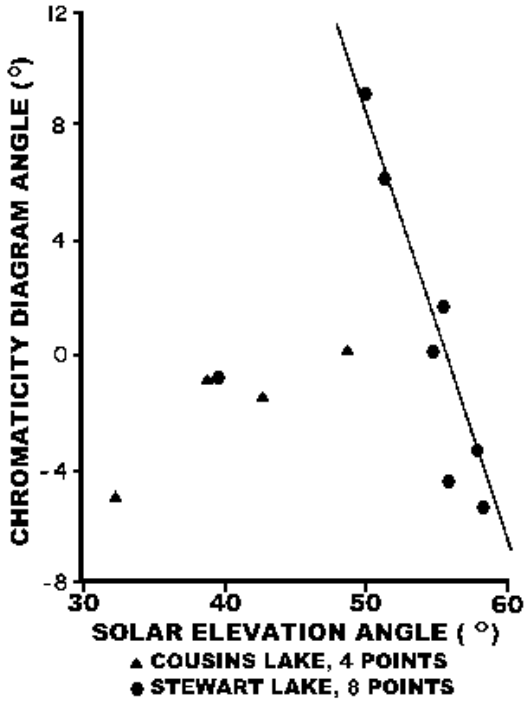

Figure 11. Solar Elevation Angle Versus Chromaticity Angle for Two Oligotrophic Lakes. Stewart Lake point near Brewster's angle (36.9^0) omitted from regression.

all regressions were repeated omitting this point. Angle θ_E then produced a correlation coefficient of 0.950 ($P < 0.001$). At the same time, the correlation coefficient for d against solar angle produced a negligible $r = 0.09$. The omitted data point is from the date with the lowest solar angle (36.5^0, which is 11^0 smaller than any of the other dates). Generally, the surface reflection of low angle sunlight increases smoothly, and the subsurface refraction angle (relative to the nadir) increases smoothly, as the solar elevation angle decreases; these changes should gradually, not sharply, alter the Landsat chromaticities. However, the given angle, unlike the others, is slightly below the Brewster angle for water, 36.9^0 at 15^0C. The Stewart Lake results indicate that, above the Brewster angle, solar angle variations cause a swing of chromaticities around E, without affecting the radial distance from E which was earlier shown to measure the interference of the atmosphere.

For Cousin's Lake only θ_E was weakly correlated with solar angle ($r = 0.900$, $n = 4$, $P < 0.1$). Two of the four points are near or below the Brewster angle.

At northern latitudes, solar elevation angles for Landsat passes can be below the Brewster angle for five months of the year. In such instances, sea state variations producing wave angles on both sides of the Brewster angle might introduce considerable noise to S measurement. However, in winter months with low solar angles, northern lakes are frozen and thus inaccessible by Landsat.

The results suggest that solar angle effects on S measurement by chromaticity analysis are negligible. A second order chromaticity correction for solar angles larger than the Brewster angle could be accomplished by application of a regression such as shown in Figure 11. Also, Landsat data may be noisy for solar elevation angles below the Brewster angle.

SECCHI DEPTH AND TURBIDITY

Some water quality monitoring agencies still find it convenient to characterize water bodies by Secchi Disc depth and various other measures of 'turbidity" or "water clarity", in stead of by suspended sediment concentration in mg/l. Recently, the U.S. Geological Survey has recommended that the use of turbidity measures be discontinued altogether (see Pickering, 1976). However, it is likely that the use of Secchi disk depth and other measures of turbidity will continue indefinitely. The question then arises whether the chromaticity system can be used to measure these variables.

Regression of chromaticity coordinates against Secchi disk depth for several sets of data in the literature produces high correlation coefficients (see Table 5). In these data sets, the correlations using chromaticity coordinates are as high or higher than those based on single MSS bands or on MSS band ratios. Also, a correlation will usually be found between suspended solids and some measure of turbidity, for example, Scherz, *et al*. (1973, Figure 7), where the correlation is between suspended solids and Jackson Turbidity Units. Hence, the indications at present are that the Landsat chromaticity system will be useful for multitemporal measurement of Secchi disk depth and turbidity.

SYSTEM APPLICATION IN THE BAY OF FUNDY TIDAL POWER PROJECT

The Nature of the Application

The Bay of Fundy, because of its large tidal range, is being considered for Tidal Power Development (Atlantic Tidal Power Programming Board, 1969; Bay of Fundy Tidal Power Review Board, 1977). This involves constructing a barrage across the tidal flow, thus creating a headpond, then generating energy by feeding water from the headpond to the sea during periods of low tide. The headpond is subsequently filled on the following high tide. Though simple in principle, the project is an enormous undertaking estimated to cost $4 billion.

Owing to the asymmetric nature of tides and tidal currents in nearshore regions, suspended sediment is concentrated in the headward regions of estuaries (Postma, 1961). Figure 12, a photograph of the Bay of Fundy taken from Skylab during September 1973, clearly shows

Figure 12. A photograph of the Upper Bay of Fundy Taken From Skylab During September 1973 (original in colour). The image shows the progressive increase in S headwards, the general circulation pattern of the water, and the turbid "boils" in Minas Basin associated with turbulence.

the headward increase in S and the silty nature of the Bay's waters. All three principal sites being considered for the Tidal Power Development are in the regions of high S (see Figure 3).

With constant supply, S is predominantly a function of current speed (A.S.C.E., 1975). If tidal currents are inhibited, or energy removed from the flow, the competency and capacity of the flow is reduced and siltation will occur. In the Wash, East England, rapid siltation has taken place immediately seawards of reclamation embankments and entraining walls constructed in the tidal flows (Kestner, 1975; Inglis and Kestner, 1958). The amount of siltation is proportional to the reduction in current speed. In the upper Bay of Fundy, dramatic accumulations of mud have developed to the seawards side of rock fill causeways built across tidal channel ways (Amos,

1979). These causeways have completely altered the tidal flow and as a result, the original tidal channels have diminished to small creeks which are flushed by outflowing river water.

It appears reasonable to assume that siltation will result from Fundy Tidal Power development. The question is where and how much siltation will occur, and also, what will its impact be on the efficiency and lifetime of the power plant. Answers have been provided by a predictive numerical model of the Fundy system (Greenberg and Amos, in preparation.; Greenberg, 1977) which has been initialized and calibrated from maps of suspended sediment concentration derived from chromaticity analysis of Landsat data.

Contour Maps of S

The preceding discussions show the validity of extrapolating the calibration shown in Figure 4 outside the immediate region of the calibration to produce contour maps of S for the entire upper Bay of Fundy. The Minas Basin region constitutes an area of 1,100 km^2 and is represented by 0.25 x 10^6 Landsat pixels. For several overpasses, contour maps were produced as shown in Figures 13 and 14. The contour intervals chosen are in $\log_e$ progression which appears

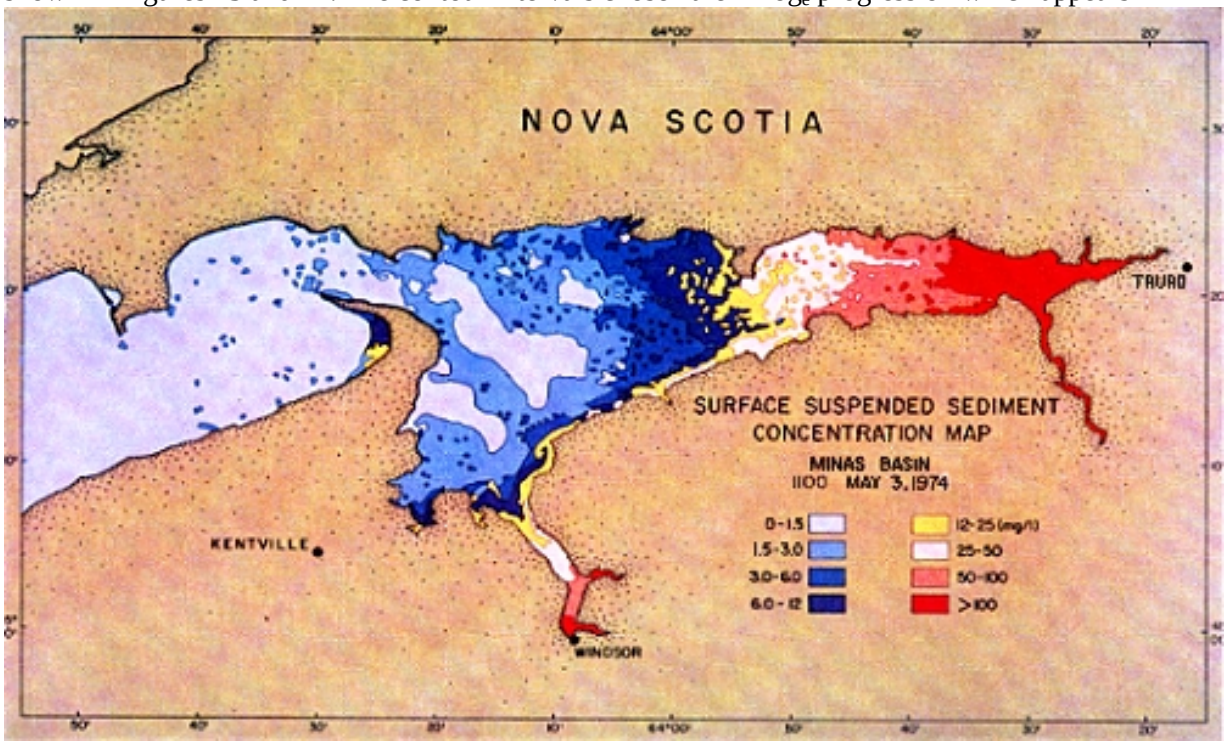

Figure 13. Thematic Map of S in Minas Basin Derived From Chromaticity Analysis of Landsat Digital Data. 1430 GMT, May 3, 1974, 0.5 hr. after high water. The contours show the clearer water at the centre of a clockwise gyre in central Minas Basin, the general increase in S headwards through the system, and the seaward movement of sediment along the south shore of Minas Basin. The instantaneous volume of sediment was estimated to be 0.25 x 10^6 m^3 and was determined by integrating the S levels with depth.

to give an even spatial distribution of contours. Such a distribution is useful for interpreting mass water movement. However, for pattern identification or for calculations of the mass of suspended sediment, a linear progression is more appropriate.

A series of S contour maps was produced for differing weather conditions for each season and at various stages of the tide. Residual tidal circulation patterns were identified from the

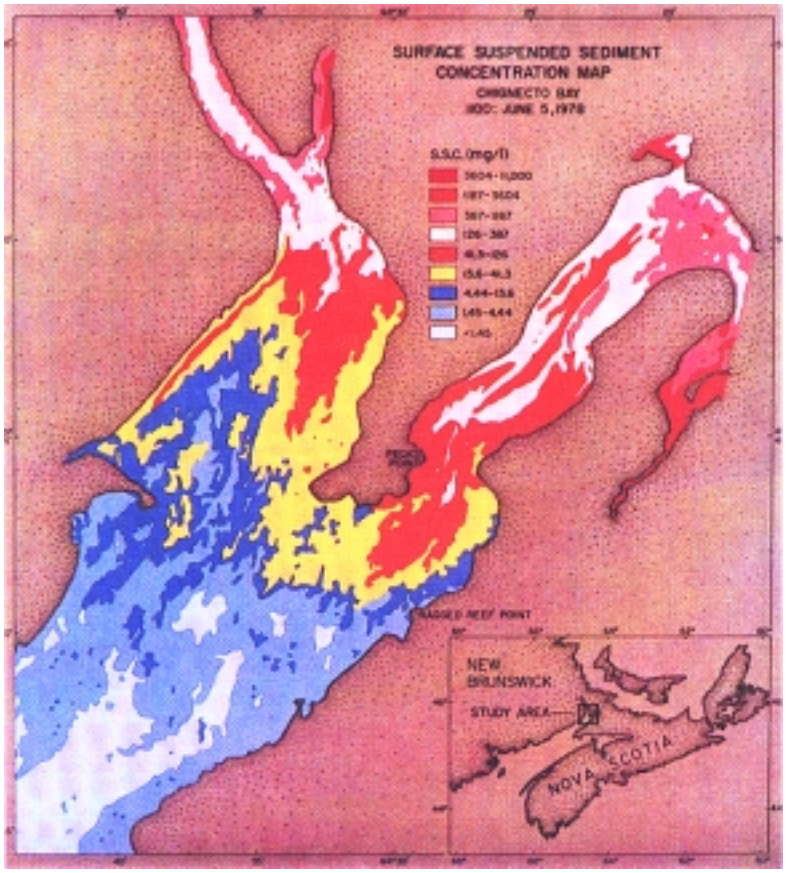

Figure 14. Thematic Map of S in Chignecto Bay From Landsat Data. 1500 GMT, June 5, 1978, 1.5 hrs. before high water. Tidal currents approximately 2 m/sec. moving from bottom to top of the image.

inflections of the contours, and verified by comparison to tidal flow models of Tee (1977) and Greenberg (1977). The contours in Figure 13 represent conditions during May 4, 1974, one half hour prior to high tide. The north shore of Minas Basin appears flood dominant and the south shore ebb dominant. The lobes and saddles of the contour lines show clearly the seaward transport of material along the south shore, a phenomenon which prior to this time had not been identified, and the movement of clearer offshore waters along the north shore. A total load of 0.25 x 10^6 m^3 of suspended particulate matter was estimated to be in suspension. Calculations were made by integrating the surface S distribution with depth, having previously determined the vertical distribution (Amos and Joice, 1977). During conditions of the highest S, 12 x 10^6 m^3 of material were in suspension.

The maps show that the highest S values occur during the spring. The average S in the central part of the basin in this season is approximately 60 mg/l. Lowest values occur during the summer (1-5 mg/l), and intermediate concentrations occur during the winter and autumn (40 mg/l). It is significant that the ice-free pattern of contours (at any particular stage of the tide) does not change. This indicates that the various sediment transport processes change only in magnitude and not in their spatial distribution.

The significance of these calculations is in the prediction of siltation associated with the Fundy Tidal Power Project. The masses of material determined from the maps of S clearly show the need for an analysis of post-barrage sedimentation patterns. Therefore, spring maps were used to initiate a numerical simulation model (Greenberg, 1977) and simulate the most intense conditions of sedimentation which could result. The model was then adjusted until, after a series of tidal cycles, it approached summer conditions of sediment transport, distribution and deposition. The ebb transport in Figure 13 was used as a criterion for evaluating the model

simulation which is shown in Figure 15 after having been run for 7 tidal cycles. The pattern of S contours agreed markedly with those generated by the satellite data.

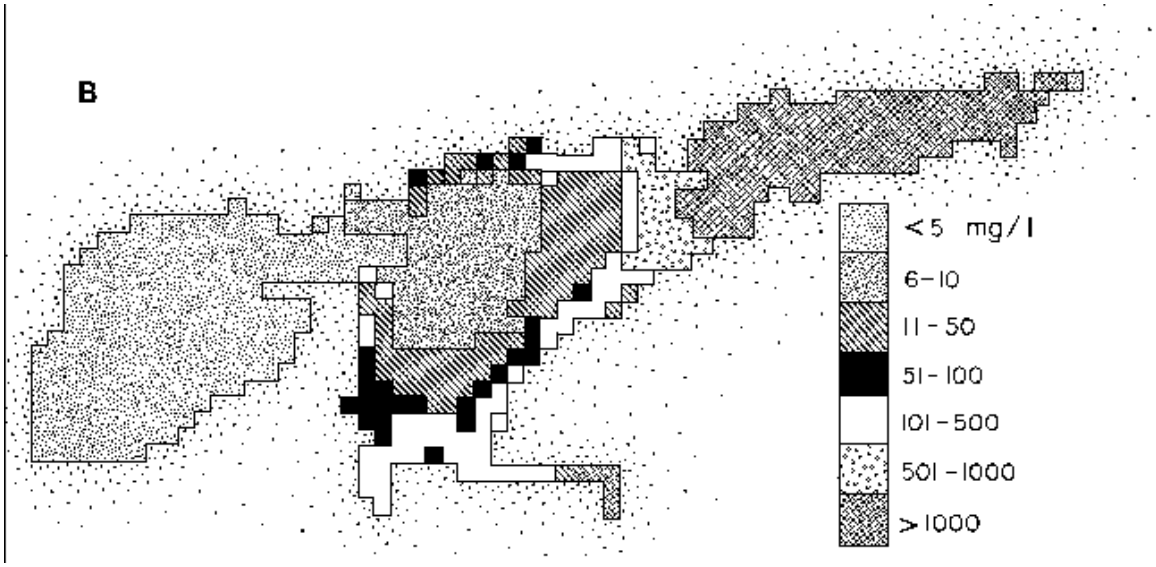

Figure 15. Simulation of Suspended Sediment Distribution From the Greenberg Numerical Model (1977). After the passage of 7 tidal cycles following the Figure 13 condition. The simulation represents the high tide condition. Notice the similarity in S contour distirubution to Figure 13 and the presence of the seaward residual of sediment along the south shore.

Basco, *et al*. (1974), in summarizing the field of sedimentation theory, stated that predictive numerical models of sedimentation are only as valid as the boundary conditions and calibration of the model. The application of S maps to the calibration and running of the model unquestionably improved its validity.

The results from the Bay of Fundy model, run with a barrage term, show that only minor amounts of sedimentation within the headpond region will result; the lifetime expectancy (based purely on sediment deposition) will not be affected. This is a rather significant conclusion for the operation of the Tidal Power scheme, and is based in part on the information derived from the Landsat MSS.

S Patterns Derived From the Contour Maps

The spatial distribution of S at the head of the Bay of Fundy is often not regular, but shows a series of distinct patterns on the Landsat images and S contour maps. These patterns develop as a result of local irregularities in seabed morphology, channel shape, and water depth, which in turn induce hydraulic irregularities on a local scale. Where such irregularities of flow do not exist, the simplest case of regular headward increase in S is to be expected (illustrated in Figure 16A). The S contours are then straight and normal to the direction of flow. Cobequid Bay in the Minas Basin demonstrates this pattern in general; however, irregularities of tidal flow have distorted the S contours into a series of saddles and lobes.

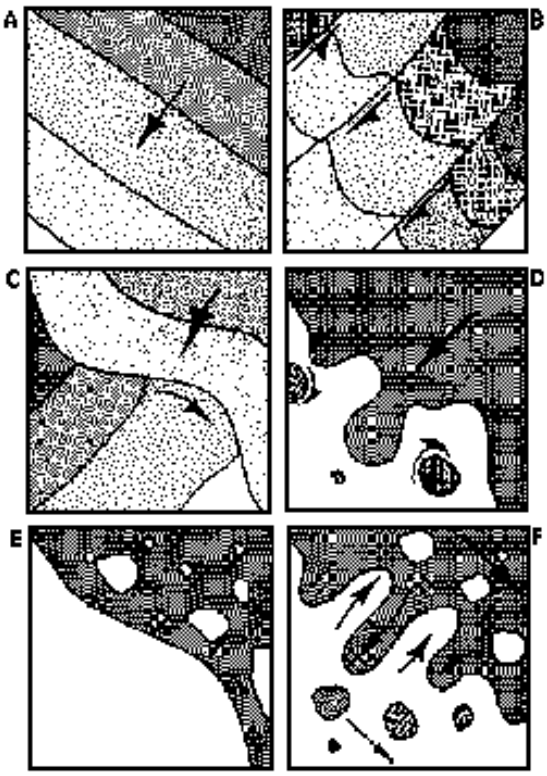

Figure 16. Schematic Illustrations of S Contour Patterns Which Occur in the Bay of Fundy: (A) a regular gradation from high (darker) to low (lighter) S levels, contours are regular. (B) lateral shearing causes tidal water to flow in parallel, distinct ribbons, each with an independent S gradient and a different speed. (C) the boundary of two water masses moving at 90^0 to one another developed at the confluence of two tributaries. The flow of the lower water mass predominates. (D) an S contour under accelerating tidal currents. Turbulences "burst" to the surface in boils carrying sediments within them. (E) an S contour under dwindling tidal currents. Sediment at higher S levels settles out at higher rates, causing the S gradient to distintegrate. (F) an S contour along the shear zone of two water masses moving in parallel. Lateral exchange of sea water and sediment cocurs due to differential current speeds between the two water masses.

In Chignecto Bay, lateral irregularities in bathymetry and inertial effects of flow cause the tidal water to shear into a number of water masses. These masses move parallel to one another but at different speeds. They are separated by narrow shear zones and are identified by markedly different concentrations of sediment. Figure 16B illustrates the S distributions developed under such conditions. The catenary pattern develops from a series of isolated S gradients within each of the "ribbons" of the tidal flow. This phenomenon demonstrates the problem of representative sampling in tidal regions, and the inherent errors involved in laterally extrapolating data from one point of a channel to define the total cross section. Mass transport calculations through channels subject to this type of flow cannot be made without representative sampling within each water mass.

Waters ebbing through the confluence of two tidal estuaries, converging at a high angle, tend not to mix. Usually, the flow with the greatest momentum displaces that with the lesser to produce a situation illustrated in Figure 16C. Here, the main flow is across the bottom of the diagram and the subsidiary flow is across the top. Two S gradients are developed oblique to one another, and an unconformity is developed at the junction of the two water masses. This is a short lived phenomenon, occurring during an ebbing tide, and has been seen in the Petitcodiac River and Avon River estuaries.

The S levels are controlled principally by the magnitude of the tidal currents, which vary, accelerating and decelerating over a tidal cycle (Amos and Long, in press). During the phase of acceleration, material is swept into suspension by "boils" of turbulence. Such turbulent "boils" can be seen in Figure 12, and are illustrated in Figure 16D. Zones of turbid boils are found intruding into water masses generally characterized by lower S values. The S contours are convolute or often diffused and difficult to identify.

During phases of dwindling currents, when turbulence is low enough to allow sediment settling, the water begins to clear. The rate of clearing depends on the initial concentration, the particle settling rate, and the current shear velocity relative to the critical settling shear velocity (A.S.C.E., 1975). In the Bay of Fundy, settling varies on a pixel level, regions of clearer water appearing in more turbid zones in response to localized dynamic conditions. This phenomenon has been observed to take place after storms or periods of high wave activity at either high or low tide, and is illustrated in Figure 16E.

The final example, illustrated in Figure 16F, shows mass transport of water and sediment, either through a shear zone separating two water masses, or across contour levels. This mass exchange of water occurs typically on a pixel level. It can result from eddying of a shear zone separating two water masses, or through down current irregularities of flow. The resulting S pattern is typical in regions of strong currents. Examples can be seen in the colour map of Chignecto Bay, shown in Figure 14. The scene was recorded by Landsat on June 5, 1978, 1.5 hours before high tide, during which time the currents were flowing at approximately 3 m/sec.

CONCLUSIONS

An automated system for quantitative measurement of suspended sediment concentration from Landsat MSS CCT data is now operational. Based on chromaticity analysis, the system permits the surface calibration data of one satellite scene to be applied to another, by an adjustment which accounts for variations in atmosphere, water surface geometry, and solar angle. The technique has been verified using nine data sets with a total of 108 points from the Bay of Fundy in Eastern Canada. Correlation between satellite and surface data for the combined data sets (after relative atmospheric adjustments) is 96 percent and the absolute error of the calibrated satellite measurements is approximately 44%.

The system has been applied to the Fundy Tidal Power Project, to initialize and calibrate a Bay of Fundy numerical model. This model indicates that no significant sedimentation is to be expected from the proposed tidal barrage during the design lifetime of the project, confirming the viability of the tidal power plan.

ACKNOWLEDGMENTS

We thank P. Manuel and H. Gordon for data reduction; J. VanGulik for programming; and D. Schultz and L. Marshall for typing. L.C.M. partially supported by NASA grant NGL 47-022-055. VIMS Contribution No. 909

LITERATURE CITED

Ahern, F.J. and J. Murphy, 1978. Radiometric Calibration and Correction of Landsat 1,2, and 3 MSS Data. Research Report 78-4, Canada Centre for Remote Sensing, Energy, Mines and Resources, Ottawa

Alföldi, T.T. and J.C. Munday, Jr. 1977. Progress Toward a Landsat Water Quality Monitoring System. Proc. 4th Canadian Symp. Remote Sens., Quebec City, pp. 325-340

Alföldi, T.T. and J.C. Munday, Jr. 1978. Water Quality Analysis by Digital Chromaticity Mapping of Landsat Data. Canadian Journal of Remote Sensing, 4(2): 108-126

American Society of Civil Engineers. 1975 Sedimentation Engineering, V.A.Vanoni, (Editor.), 54, 745p.

Amos, C. L. 1976. Suspended Sediment Analysis of Sea Water Using Landsat Imagery, Minas Basin, Nova Scotia. In Report of Activities, Part C. Geological Survey of Canada, Paper 76-1C, pp. 55-60

Amos, C. L. 1979. Sedimentation Resulting from Fundy Tidal Power. In Tidal Power and Estuary Management, Severn, R. T., Dineley, D. L. and Hawker, L. E. (Eds.), Publ. Colston Research Society, p. 173-179

Amos, C. L. and T. T. Alföldi 1979. The Determination of Suspended Sediment Concentration in a Macrotidal System Using Landsat Data. J. Sedim. Petrol., 49: 159-174

Amos, C. L. and G.H.E. Joice. 1977. The Sediment Budget of the Minas Basin, Bay of Fundy, Nova Scotia., Bedford Inst. Ocean. Data Series Bi-D-77-3, 411p.

Amos, C. L. and B.F.N. Long (in press). The Sedimentary Character of the Minas Basin, Bay of Fundy, Proc. Coastlines Canada Conf., Halifax, N.S.

Atlantic Tidal Power Programming Board. 1969. Report of Atlantic Tidal Power Programming Board on the Feasibility of Tidal Power Development in the Bay of Fundy, Halifax, Nova Scotia, Unpublished Report.

Basco, D.R., A.H. Bouma, and W.A. Dunlap, 1974. Assessment of the Factors Controlling the Long-Term Fate of Dredging Material Deposited in Unconfined Subaqueous Disposal Areas. Dredged Material Research Program Report D-74-8, 238 pp.

Bay of Fundy Tidal Power Review Board. 1977. Reassessment of Fundy Tidal Power. Publ. Thorn Press Ltd., Ottawa, Ontario, 516 pp.

Bernstein, R. 1978. Digital Image Processing of Earth Observation Sensor Data. In: Digital Image Processing for Remote Sensing, R. Bernstein, (Editor). IEEE Press pp. 55-72.

Boland, D.H.P., 1976. Trophic Classification of Lakes Using Landsat-1 (ERTS-1), Multispectral Scanner Data, U.S. Environmental Protection Agency, EPA-600/3-76-037, Cornwallis, Oregon, 140pp. And app.

Bowker, D.E, W.G. Witte, P. Fleischer, T.A. Gosink, W.J. Hanna and J.C. Ludwick. 1975. An Investigation of the Waters in the Lower Chesapeake Bay. Proc. 10th International Symposium, Remote Sensing of Environment. Env. Res. Inst. Michigan, Ann Arbor, pp. 411-420

Bukata, R.P., G.P. Harris and J.E. Bruton. (1974). The Detection of Suspended Solids and Chlorophyll “A” Utilizing Digital Multispectral ERTS-1 Data. Proc. Second Canadian Symposium on Remote Sensing, Vol 2, p. 551-564

Folk, R.L., 1968. Petrology of Sedimentary Rocks. Univ. Texas, Austin, 170 pp.

Greenberg, D. 1977. Effects of Tidal Power Development on the Physical Oceanography of the Bay of Fundy and Gulf of Maine. In: Fundy Tidal Power and the Environment, Daborn (Editor), Acadia Inst., p. 200-232.

Greenberg, D. and C.L. Amos (in preparation). The Numerical Simulation of Suspended Sediment Transport and Deposition Associated With Fundy Tidal Power, Minas Basin.

Holyer, R.J. 1978. Toward Universal Multispectral Suspended Sediment Algorithms. Remote Sensing of Environment, 7: 323-338

Inglis, C.C. and F.J.T. Kestner, 1958. The Long-Term Effects of Training Walls, Reclamation, and Dredging on Estuaries. Proc. Civil Engrs. 9:193-212.

Jerlow, N.G. 1976. Marine Optics. Publ. Elsevier Oceanog. Ser. 14, 231 pp.

Kestner, F.J.T. 1975. The Loose-Boundary Regime of the Wash. Geogr. J., 141: 389-412

MacIntosh, Ml, J.D. Willey, and C. Courneya, 1976. A Compendium of Sampling and Analytical Techniques Used by E.M.G. B.I.O. Int. Rep. Unpublished manuscript.

Minnesota Region 5 Regional Development Commission, 1978. Mapping of Chlorophyll a Concentrations and Secchi Disc Depth of Lakes Within Region 5 Using Landsat Digital Data. State of Minnesota, St. Paul, 21 pp.

Munday, J.C., Jr., 1974a. Lake Ontario Water Mass Delineation From ERTS-1. Proc. 9th Intl. Symp. Remote Sensing of Environment, University of Michigan, Ann Arbor, pp. 1355-1368.

Munday, J.C., Jr., 1974b. Water Quality of Lakes of Southern Ontario From ERTS-1. Proc. 2nd Canadian Symposium on Remote Sensing, Guelph, Ontario, pp. 77-86.

Munday, J.C., Jr. and T.T. Alföldi. 1975. Chromaticity Changes From Isoluminous Techniques Used to Enhance Multispectral Remote Sensing Data. Remote Sensing of Environment. 4(3): 221-236.

Munday, J.C., Jr. and T.T. Alföldi. 1979. Landsat Test of Diffuse Reflectance Models for Aquatic Suspended Solids Measurement. Remote Sensing of Environment, 8: 169-183. Ann Arbor, pp. 1355-1368

NASA Landsat Data Users Handbook, 1976. Doc. No. 76DS4258, Greenbelt, Maryland.

Pickering, R.J. 1976. Measurement of “Turbidity” and Related Characteristics of Natural Waters. U.S. Geological Survey Open File Report 76-153, Reston, Virginia, 7pp.

Postma, H. 1961. Transport and Accumulation of Suspended Matter in the Dutch Wadden Sea. Netherlands Journal Sea Res., 1: 148-190

Rogers, R.H., N.J. Shah, J.B. McKeon, C. Wilson, and L. Reed, 1975. Applications of Landsat to the Surveillance and Control of Eutrophication in Saginaw Bay. Proceedings of the 10the International Symposium of Remote Sensing of the Environment, Environmental Research Institute of Michigan, Ann Arbor, pp. 437-446.

Rogers, R.H., N.J. Shah, J.B. McKeon and U.E. Smith. 1976. Computer Mapping of Water Quality in Saginaw Bay With Landsat Digital Data. Proc. ASP Convention (Washington, D.C.), American Society of Photogrammetry, Falls Church, Virginia, 13pp.

Scherz, J.P. (Editor) 1977. Assessment of Aquatic Environment by Remote Sensing. Institute for Environmental Studies, University of Wisconsin-Madison, 235 pp.

Scherz, J.P., M. Sydor, and J.F. VanDomelen, 1973. Aircraft and Satellite Monitoring of Water Quality in Lake Superior Near Duluth. Third ERTS-1 Symposium, NASA, Washington, pp. 1619-1636

Sokal, R.R. and F.J. Rohlf, 1969. Biometry. W.H. Freeman, San Francisco, California, 776 pp.

Strickland, J.D.H. and T.R. Parsons, 1972. A Practical Handbook of Sea Water Analysis. Fish. Res. Bd. Can. Bull. 167, 310 pp.

Tee, K.T., 1977. Tide-Induced Residual Current – Verification of a Numerical Model. J. Phys. Oceanography. 7(3): 396-402.